electronics

MDPI

Communication

A 4th-Order LTCC Bandpass Filter with Both Tunable Center Frequency and Bandwidth

Hao Wu, Bin You, Kun-Kun Gao and Xun-Gen Li *

The Key Laboratory of RF Circuits and Systems of Ministry of Education, Microelectronics CAD Center, School of Electronics and Information, Hangzhou Dianzi University, Hangzhou 310018, China
* Correspondence: lixg@hdu.edu.cn; Tel.: +86-138-6808-0672

Abstract: Reconfigurable filters are one of the key components in microwave communication systems. This letter presents a 4th-order low-temperature cofired ceramic (LTCC) bandpass filter with both a tunable center frequency and bandwidth. This filter has four resonators, and each resonator consists of a circular patch, a center-through via, and two varactors. The varactors are placed on the top and bottom layers of the ceramic medium, which can effectively reduce the size of the 4th-order tunable filter. Three transmission zeros (TZs) are introduced to improve the upper stopband rejection. This filter demonstrates a 3-dB bandwidth (BW) range of 170–220 MHz around 2.86 GHz and a 3-dB BW range of 190–320 MHz around 3.2 GHz with a 13 dB minimum return loss. Insertion loss ranging from 3.5 dB to 6.85 dB has been obtained. The overall circuit size, including the package, is 11 mm × 6 mm × 1.6 mm.

Keywords: tunable bandpass filter (BPF); low temperature cofired ceramic (LTCC); miniaturized filter; transmission zero (TZ)

Citation: Wu, H.; You, B.; Gao, K.-K.; Li, X.-G. A 4th-Order LTCC Bandpass Filter with Both Tunable Center Frequency and Bandwidth. *Electronics* **2022**, *11*, 4119. https://doi.org/10.3390/electronics11244119

Academic Editor: Alejandro Melcón Alvarez

Received: 1 November 2022
Accepted: 9 December 2022
Published: 10 December 2022

1. Introduction

With the rapid development of mobile communications, spectrum resources are becoming more and more scarce. In general, filter banks with multiple switches and fixed filters are used to adapt the communication system to different spectral environments. This method will undoubtedly increase the size, loss, and cost of the system, so high-performance reconfigurable filters have become the main research direction.

At present, most of the reconfigurable filters adopt planar or SIW cavity structures, which have large sizes. Low-temperature cofired ceramic (LTCC) technology is one of the most effective ways to achieve miniaturization, high integration, and three-dimensionalization of electronic products. Due to the small size of the LTCC filter, there is almost no space for tuning components. Few tunable filters are designed based on LTCC. Two LTCC tunable active filters with multilayer structures have been proposed in [1]. In this paper, tunable LTCC filters with varactors on the surface appear for the first time, and bandwidth-tunable LTCC filters have been developed at 400 and 800 MHz frequency bands. Beyond that, most tunable LTCC filters only realize an adjustable center frequency [2–4]. M. Rahaman reports a 3rd-order filter with combline topology for a mobile handset application [2]. J. C. Estes presents a tunable bandpass filter with practically constant bandwidth [3]. However, the LTCC filter had not been fabricated, and they used a bread-boarded, three-pole design using the filter tuning technique to test. An axial coupling structure is proposed to realize a wide tuning bandwidth [4]. In addition, some scientists have already realized tunable filters based on coaxial cavities in other process techniques [5–8]. In [8], a frequency-tunable LTCC coaxial SIW filter with a constant passband was proposed. However, it uses an SIW structure and still has a large size.

In this letter, a compact 4th-order LTCC bandpass filter with both a tunable center frequency and bandwidth is proposed, which has three TZs to improve the upper stopband rejection.

2. Analysis of the Tunable LTCC Bandpass Filter

The 3-dimensional structure of the proposed LTCC filter is shown in Figure 1. The filter consists of nine metal layers and sixteen ceramic dielectric layers. The top and bottom layers mainly host I/O ports and tunable components. In the second and eighth layers, there are two short microstrip lines $P_{S\text{-}L}$ with a length of $L_{S\text{-}L}$ to generate the source-load coupling for skirt selectivity improvement. As shown in Figure 1, Layers 3–7 form the four resonators, which consist of metal via holes and circular patches. Layers 4, 5, and 6 are the ground planes.

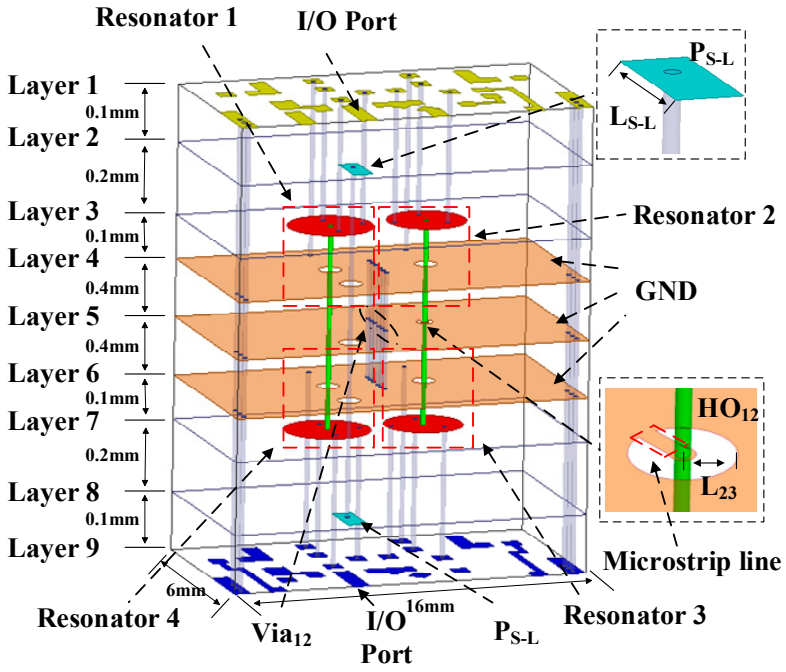

Figure 1. The 3-dimensional structure of the proposed LTCC filter.

Between the four resonators, there is a row of metal via holes (Via_{12}) connected to the ground to control the coupling strength between the resonators in the same layer. Resonators 2 and 3 are coupled through the hole (HO_{12}) in layer 5, and the coupling strength can be adjusted by the radius L_{23}. Meanwhile, these two resonators are connected to a ground by a microstrip line of length L_{23}, which decreases the resonant frequency. In this design, the radii of the circular patch in resonators 1 and 4 are larger than those in resonators 2 and 3 to compensate for frequency offset.

The top and side views of the proposed tunable resonator are illustrated in Figure 2. The resonator mainly consists of a circular patch (P_1), a center via (VI_1), and two varactors. The varactor is used to tune the resonant frequency of the resonator. H_1 is the distance from P_1 to the ground. R_4 and L_{15} represent the radius of P_1 and the length of VI_1, respectively.

Figure 3 shows the equivalent circuit of the proposed resonator. The cavity, which is filled with LTCC, is equivalent to a capacitor, and the through-metal via is equivalent to an inductor [9]. The equivalent capacitance between the circular patch and ground is C_g and the equivalent inductance of the center via is L_{vi1}. The equivalent inductances of the via holes connected to the varactor are L_{vi2} and L_{vi3}.

From Figure 3, the input admittance (Y_{in}) of the equivalent circuit can be calculated as:

$$Y_{in} = \frac{\omega^4 C_g C_3 L_{vi1} L_4 - \omega^2 (C_g L_{vi1} + C_3 L_4 + C_3 L_{vi1}) + 1}{j\omega L_{vi1} (1 - \omega^2 C_3 L_4)} \quad (1)$$

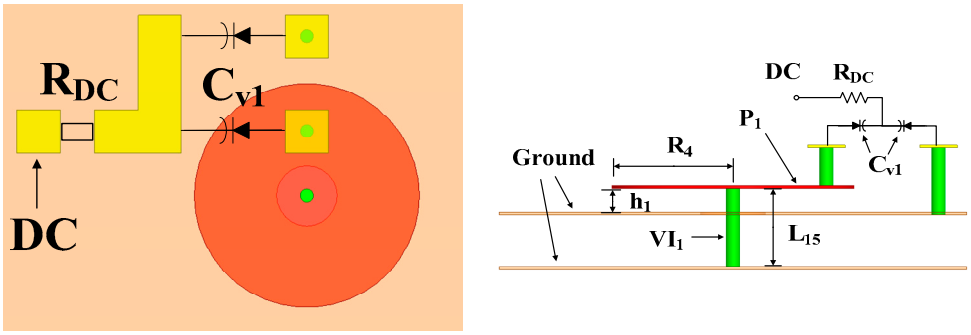

Figure 2. Schematics of the proposed tunable resonator: (**a**) top view; (**b**) side view.

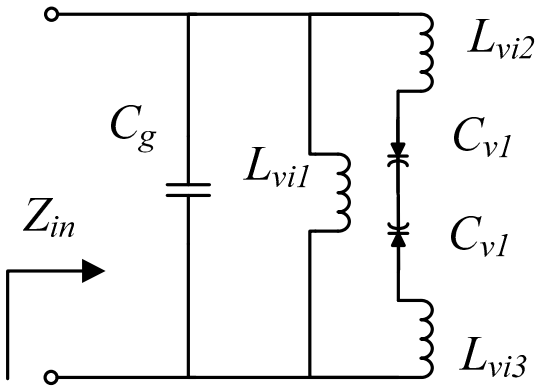

Figure 3. The equivalent circuit of the proposed resonator.

By calculating $Y_{in} = 0$, the resonant frequency can be obtained as:

$$\omega_0 = \sqrt{\frac{b - \sqrt{b^2 - 4a}}{2a}} \tag{2}$$

where

$$a = C_g C_3 L_{vi1} L_4,\ b = C_g L_{vi1} + C_3 L_4 + C_3 L_{vi1} \tag{3}$$

$$C_3 = \frac{C_{v1}}{2},\ L_4 = L_{vi2} + L_{vi3}. \tag{4}$$

From Equations (2)–(4), we can see that the resonant frequency can be determined using C_{v1}, C_g, L_{vi1}, L_{vi2}, and L_{vi3}. As shown in Figure 4a, the resonant frequency can be tuned with C_{v1}. Moreover, with the increase in the R_4 and L_{15}, the resonant frequency decreases. Figure 4b shows the simulated *Qu* versus the resonant frequency under different parasitic resistance R_s. From Figure 4b, it can be seen that the parasitic resistance R_s of the varactor has a great influence on the unloaded quality factor of the resonator.

Figure 5 shows the coupling schematic, where the capacitance values of C_{v12} and C_{v34} are the same. The coupling coefficient K, including electrical coupling k_e and magnetic coupling k_m, can be expressed with Equation (5):

$$K = k_m + k_e \tag{5}$$

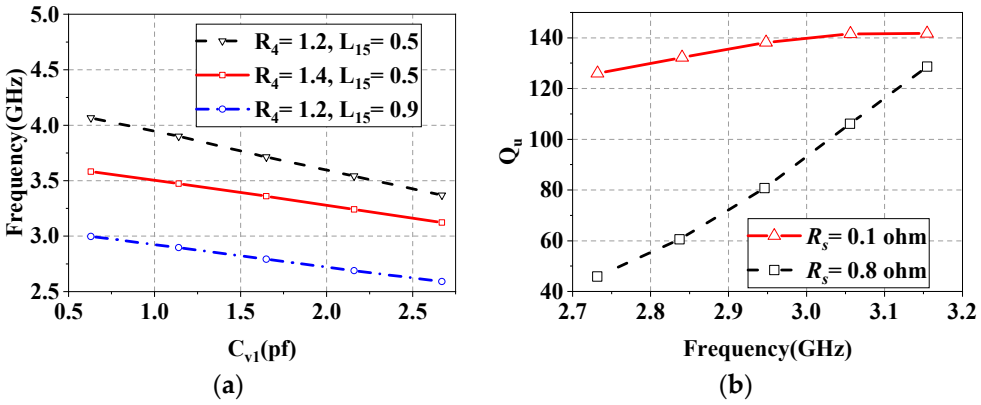

Figure 4. (**a**) The resonant frequency of resonators versus C_{v1} for different R_4 and L_{15}. (**b**) Simulated Qu versus the resonant frequency; R_s is the parasitic resistance of C_{v1}.

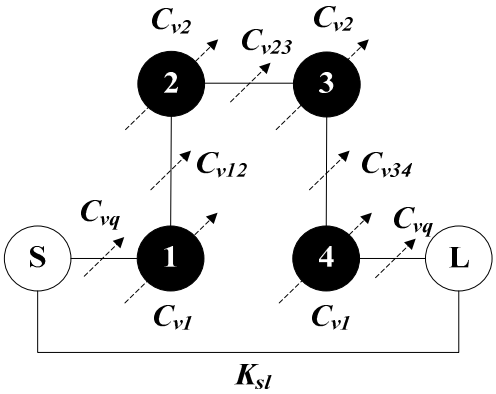

Figure 5. Coupling schematic for the proposed filter.

We set the sign of magnetic coupling as negative and that of electric coupling as positive.

Figure 6 shows the coupling structure between resonators 1 and 2. The d_{12} is the distance from the center line of the resonators 1 and 2 to Via_{12}, which can influence the electrical coupling coefficient K_{12}. Figure 7 shows the coupling structure between resonators 2 and 3. K_{23} is the magnetic coupling coefficient, which can be changed by the parameter L_{23}, and also can be tuned with C_{v23}.

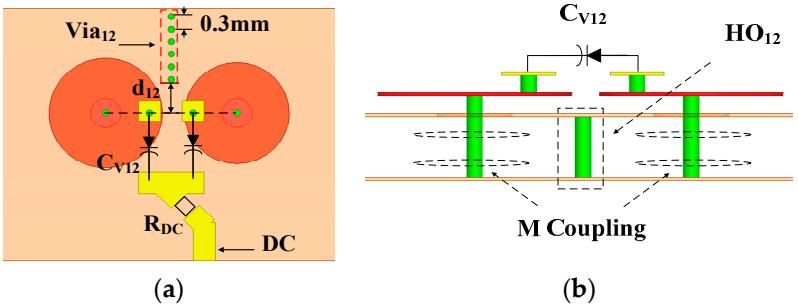

Figure 6. The coupling structure of resonators 1 and 2: (**a**) top view; (**b**) side view.

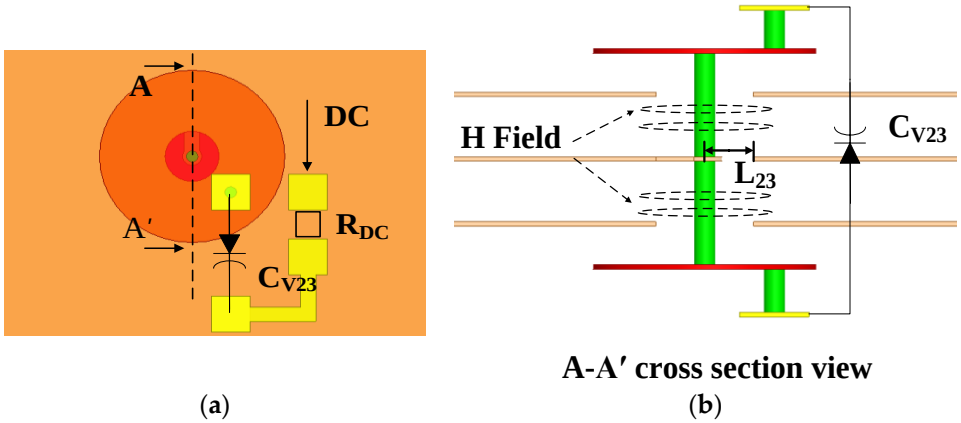

Figure 7. The coupling structure of resonators 2 and 3: (**a**) top view; (**b**) side view.

Figure 8 shows the relationship between K_{12} and C_{v12} under the different d_{12}. When $C_{v12} < 0.59$ pf, the mixed coupling coefficient $K_{12} < 0$. Further, the main coupling is magnetic coupling. With the increase in capacitance C_{v12}, the coupling coefficient K_{12} is positive and electrical coupling is the main coupling. The relationship between K_{23} and C_{v23} under the different L_{23} is also shown in Figure 8. It can be seen that K_{23} can be tuned with the C_{v23} and its tuning range can be controlled with the L_{23}.

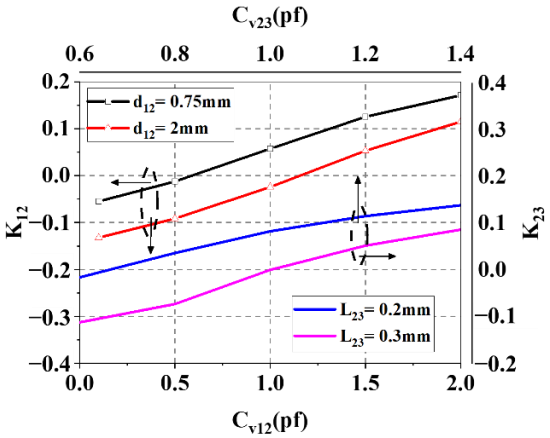

Figure 8. K_{12} versus Cv_{12} for different d_{12} (left). K_{23} versus Cv_{23} for different L_{23} (right).

The structure of the I/O port is illustrated in Figure 9a. The I/O ports are connected to the resonator through a capacitor (C_1) and a varactor (C_{vq}). As can be seen from Figure 9b, the external Q value Q_e will decrease with the increase in C_{vq}, when C_{v1} is fixed. As shown in Figures 1 and 9a, the microstrip line $P_{S\text{-}L}$ is used to generate the source-load coupling, so the length $L_{S\text{-}L}$ of the microstrip line can be used to tune the position of TZs.

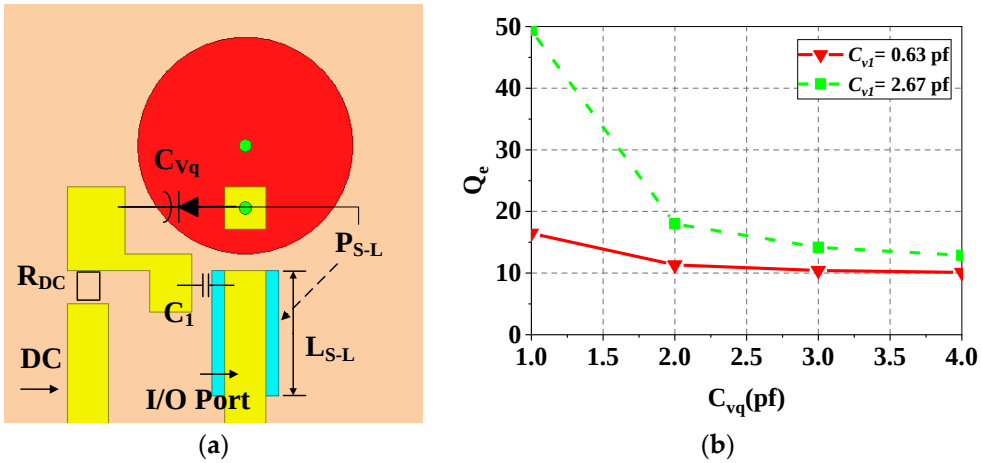

Figure 9. (**a**) Top view of the structure of the I/O port. (**b**) Simulated Q_e versus C_{vq} for different C_{v1}.

3. Experimental Results

To verify the accuracy of the above design, a four-pole tunable LTCC filter is fabricated, and the layouts are shown in Figure 10. Layers 6, 7, and 8 are the same as layers 4, 3, and 2. The dielectric constant of the LTCC substrate is 7.5, and the loss tangent is 0.006. The test circuit board is Rogers 4003C. There are 16 varactors loaded on the surface of the proposed filter, and their models are SMV1405 (C_{v1}, C_{v2}, C_{v12}, C_{v34}), SMV1413 (C_{vq}), and SMV2020 (C_{v23}), respectively. The R_{DC} is 100 k ohm, and the C_1 is 3pf. The locations of the lumped elements are shown on layers 1 and 9 in Figure 10. Table 1 shows the dimensions of the designed filter. Figure 11 shows the photo of the proposed filter. The overall circuit size, including the package, is 11 mm × 6 mm × 1.6 mm.

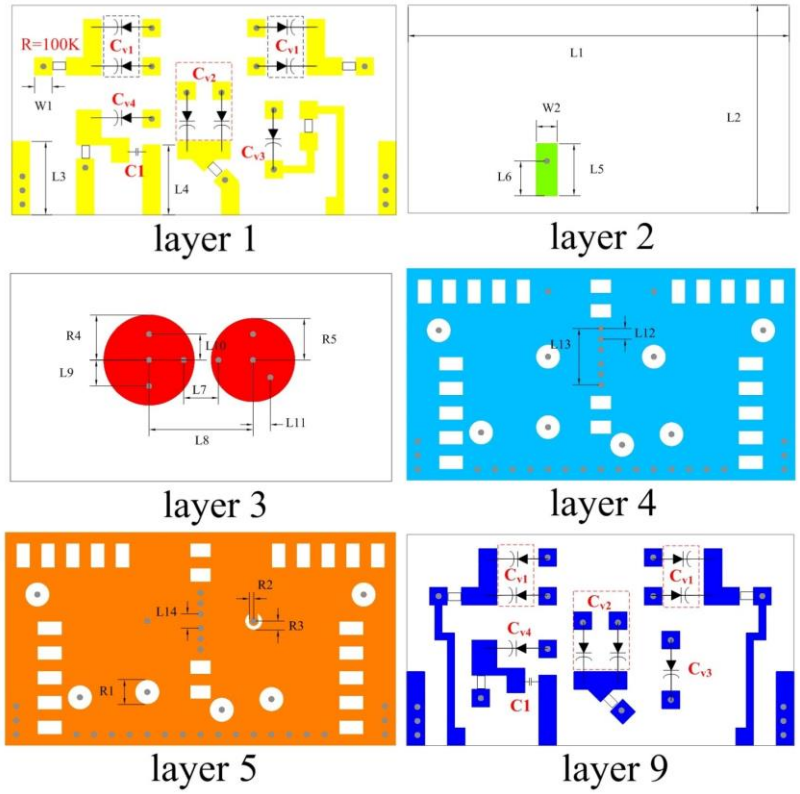

Figure 10. Layouts of the proposed LTCC filter.

Table 1. The dimensions (mm) of the designed filter.

L1	L2	L3	L4	L5	L6	L7	L8	L9	L10	L11
11	6	2.1	2	1.5	1	1	3	0.75	0.75	0.5
L12	**L13**	**L14**	**R1**	**R2**	**R3**	**R4**	**R5**	**W1**	**W2**	
0.3	1.6	0.4	0.7	0.125	0.25	1.3	1.2	0.5	0.6	

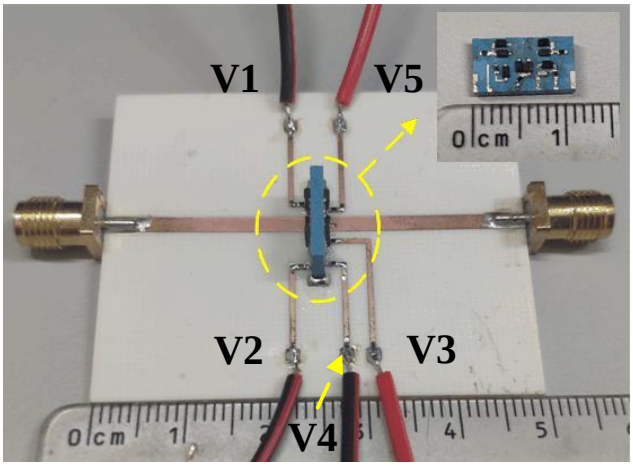

Figure 11. The photo of the proposed filter.

Figure 12 shows the measured and simulation results of the proposed filter. Only the maximum and minimum 3-dB BWs are shown at selected frequencies. The measured results and simulated results maintained a good consistency. The frequency tuning was demonstrated with a 3-dB BW ranging from 170–220 MHz around 2.86 GHz, 180–310 MHz around 3 GHz, and 190–320 MHz around 3.2 GHz. The worst insertion loss was 6.85 dB at the lowest frequency, and the return loss was better than 13 dB at all measured BWs. Insertion loss ranging from 3.5 dB to 6.85 dB was obtained. The load voltages of the varactors are given in Table 2.

Table 2. Load-voltages of varactors.

f_0 (GHz)	2.86	3.2
DC (V) Varactor (pf)	$V_1/V_2/V_3/V_4/V_5$ $C_{v1}/C_{v2}/C_{v12}/C_{v23}/C_{vqe}$	$V_1/V_2/V_3/V_4/V_5$ $C_{v1}/C_{v2}/C_{v12}/C_{v23}/C_{vqe}$
BW_{max}	1.1/2.9/2.3/7.1/0.1 2.13/1.66/1.58/0.99/5.37	5.6/31/4.5/8.2/9.8 1.05/0.46/1.25/0.79/2.57
BW_{min}	1.1/2.9/3.2/6.1/1.8 2.13/1.66/1.46/1.15/4.17	4.1/31/7.1/6.8/21.3 1.24/0.5/1.06/0.97/1.87

A comparison with selected prior works is summarized in Table 3. As can be seen, both frequency and bandwidth are tunable in the proposed filter. Additionally, compared with the 4th-order filters given in [5], the proposed filter is smaller. Since the frequency and bandwidth of the proposed 4th-order filter can be tuned at the same time, there are 16 varactors to be loaded, which makes the quality factor Q_u of the resonators lower and the insertion loss worse. In following studies, the insertion-loss performance can be improved by using a low-loss-tangent material and improving the quality factor of the varactors.

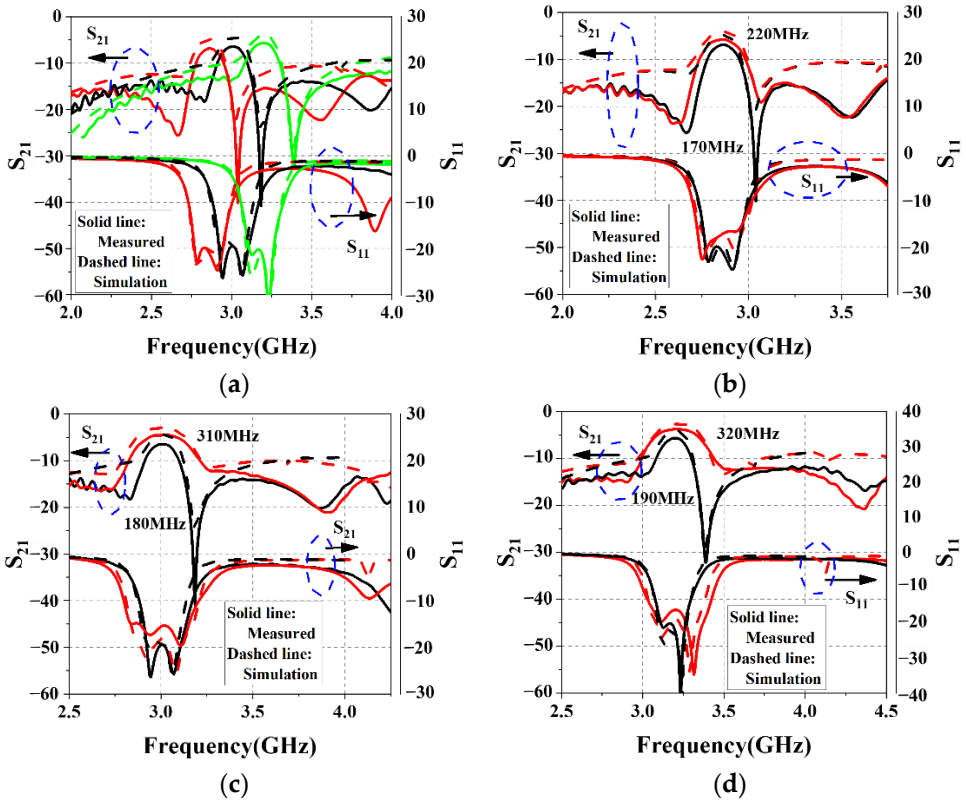

Figure 12. (**a**) The measured and simulated tuning results of the center frequency. (Red line: 2.86 GHz, Black Line: 3 GHz, Green Line: 3.2 GHz) The measured and simulated tuning results of BW at (**b**) 2.86 GHz, (**c**) 3 GHz, and (**d**) 3.2 GHz. (Red line: the maximum value of BW, Black Line: the minimum value of BW).

Table 3. Comparison with some prior LTCC filters.

	f_0 (GHz)	BW (MHz)	Filter Order	Num. of Varactors	Q_u	IL (dB)	Size (λg)
[1]	0.8–0.87	No tuning	2	2	9.8	1.4–1.8	0.041/0.041/0.018
[2]	1.71–1.98	No tuning	3	3	75.2	<4.3	0.126/0.109/0.034
[4]	0.4–0.8	No tuning	2	4	11.1	<2.65	0.107/0.080/0.043
[5]	3.9–4.57	No tuning	4	Switch tuning	180–190	1.3–1.65	0.649/0.973/0.084
This work	2.86–3.2	170–320 (max)	4	16	16.8	3.5–6.85	0.302/0.165/0.044

4. Conclusions

A 4th-order LTCC bandpass filter with both a tunable center frequency and bandwidth has been designed and manufactured. Three TZs were introduced in the stopband to improve passband selectivity. Tunable components have been placed on the surface for flexible control. The tuning ranges of the center frequency and bandwidth are 13% and 4.5%, respectively. This filter makes full use of the characteristics of the LTCC multilayer structure and greatly reduces the size of the 4th-order tunable filter compared to the filters made using other techniques.

Author Contributions: Conceptualization, B.Y. and X.-G.L.; methodology, H.W. and K.-K.G.; writing—original draft preparation, H.W. and K.-K.G.; writing—review and editing, X.-G.L. and K.-K.G. All authors have read and agreed to the published version of the manuscript.

Funding: This work was supported by the Natural Science Foundation of Zhejiang Province under Grant LZ22F010006 and the National Natural Science Foundation of China under Grant 61671195.

Conflicts of Interest: The authors declare no conflict of interest regarding the publication of this article.

References

1. Kageyama, K.; Saito, K.; Murase, H.; Utaki, H.; Yamamoto, T. Tunable active filters having multilayer structure using LTCC. *IEEE Trans. Microw. Theory Tech.* **2001**, *49*, 2421–2424. [CrossRef]
2. Rahman, M.; Shamsaifar, K. Electronically tunable LTCC based multi-layer filter for mobile handset application. In Proceedings of the IEEE MTT-S International Microwave Symposium Diges, Philadelphia, PA, USA, 8–13 June 2003; IEEE: Piscataway, NJ, USA, 2003; Volume 3, pp. 1767–1770. [CrossRef]
3. Estes, J.C. Tunable rf bandpass pass filter with variable resonator coupling. In Proceedings of the 2008 IEEE MTT-S International Microwave Symposium Digest, Atlanta, GA, USA, 15–20 June 2008; IEEE: Piscataway, NJ, USA, 2008; pp. 1035–1038. [CrossRef]
4. Zhao, B.L.; He, Z.T.; Wei, X.B.; Shi, Y. Compact tunable bandpass filter with wide tuning range and enhanced stopband characteristics. *Electron. Lett.* **2013**, *49*, 1007–1008. [CrossRef]
5. Joshi, H.; Sigmarsson, H.H.; Moon, S.; Peroulis, D.; Chappell, W.J. High-Q Fully Reconfigurable Tunable Bandpass Filters. *IEEE Trans. Microw. Theory Tech.* **2009**, *57*, 3525–3533. [CrossRef]
6. Anand, A. Reconfigurable Planar Capacitive Coupling in Substrate-Integrated Coaxial-Cavity Filters. *IEEE Trans. Microw. Theory Tech.* **2016**, *64*, 13. [CrossRef]
7. Anand, A.; Liu, X. Air Cavities Integrated with Surface Mount Tuning Components for Tunable Evanescent-Mode Resonators. In Proceedings of the 2016 IEEE MTT-S International Microwave Symposium (IMS), San Francisco, CA, USA, 22–27 May 2016; IEEE: Piscataway, NJ, USA, 2016; pp. 1–4. [CrossRef]
8. Sirci, S.; Martínez, J.D.; Boria, V.E.; Gil, J.; Marchand, L. Design of frequency tunable LTCC coaxial SIW filters with constant passband shape. In Proceedings of the 2018 IEEE MTT-S International Conference on Numerical Electromagnetic and Multiphysics Modeling and Optimization (NEMO), Reykjavik, Iceland, 8–10 August 2018; IEEE: Piscataway, NJ, USA, 2018; pp. 1–4. [CrossRef]
9. Turgaliev, V.; Kholodnyak, D.; Vendik, I.; Stöpel, D.; Humbla, S.; Müller, J.; Hein, M.A. LTCC Highly Loaded Cavities for the Design of Single- and Dual-Band Low-Loss Miniature Filters. In Proceedings of the 40th European Microwave Conference, Paris, France, 28–30 September 2010; pp. 180–183. [CrossRef]